Supplementary Information:

Nanooptics of Molecular-Shunted Plasmonic Nanojunctions

Felix Benz[1], Christos Tserkezis[3], Lars O. Herrmann[1], Bart de Nijs[1], Alan Sanders[1], Daniel O. Sigle[1], Laurynas Pukenas[2], Stephen D. Evans[2], Javier Aizpurua[3], Jeremy J. Baumberg[1,*]

[1]NanoPhotonics Centre, Cavendish Laboratory, Department of Physics, JJ Thomson Ave, University of Cambridge, Cambridge, CB3 0HE, UK

[2]Molecular and Nanoscale Physics, School of Physics and Astronomy, University of Leeds, Leeds, LS2 9JT, UK

[3] Donostia International Physics Center (DIPC) and Centro de Física de Materiales, Centro Mixto CSIC-UPV/EHU, Paseo Manuel Lardizabal 4, 20018 Donostia-San Sebastián, Spain

*Correspondence and requests for materials should be addressed to jjb12@cam.ac.uk

S1. Statistical analysis of the resonance wavelength

The distribution functions of the resonance wavelengths for all samples are shown in Fig. S1. The corresponding average resonance wavelengths are listed in Table S1.

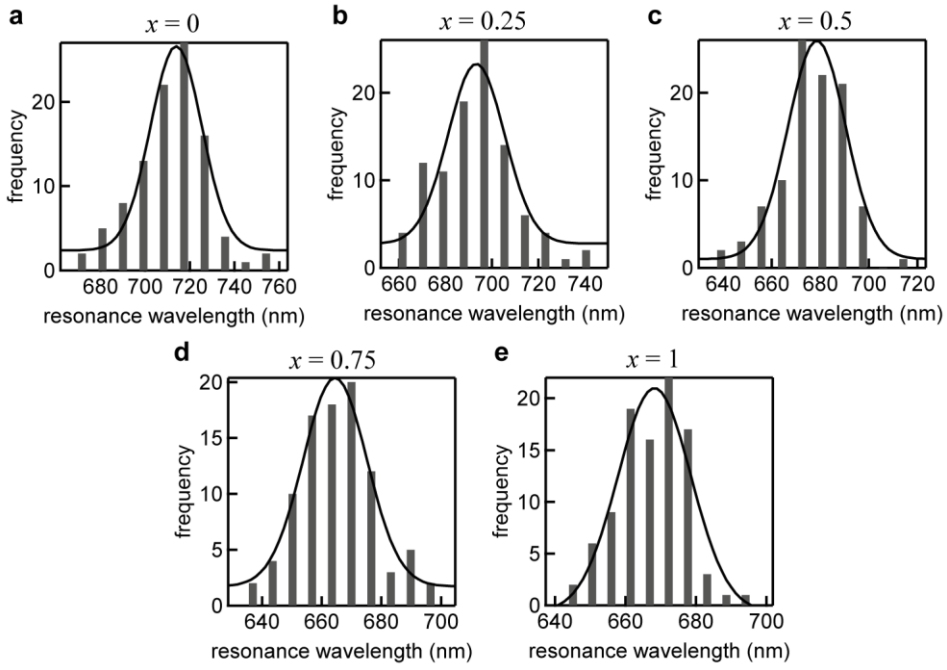

Figure S1 | Distribution functions of the observed resonance wavelengths for different SAM compositions. a to **e,** distributions for molar fractions of BPDT to BPT from 0 to 1. The black solid curves are fitted Gaussian distribution functions.

Table S1 | Observed resonance wavelengths and standard errors of the mean for different SAM compositions.

BPDT mole fraction x	resonance wavelength (nm)	± mean error (nm)
0	713.9	1.6
0.25	693.2	1.7
0.5	678.6	1.4
0.75	668.5	1.0
1	664.5	1.3

S2. Derivation of the analytical model

To calculate the fractional charge conduction $\Delta Q/Q$ due to the conducting molecules, we start by considering an arbitrary circuit element with impedance $Z = |Z| \times \exp(\mathrm{i}\theta)$. The current through such an element is:

$$I = \frac{\mathrm{d}Q}{\mathrm{d}t} = \frac{|U| \times \exp(\mathrm{i}\omega t)}{|Z| \times \exp(\mathrm{i}\theta)}. \tag{S1}$$

with voltage U on the plates. Integrating this current yields the screening charge ΔQ which should be normalised to the charge on a capacitor with the same capacity C but without a conductive link Q. Calculating the magnitude of this parameter yields:

$$\left|\frac{\Delta Q}{Q}\right| = \frac{1}{|Z|C\omega}. \tag{S2}$$

For a series capacitor and resistor we obtain for the absolute value of the impedance $|Z| = \sqrt{R^2 + {X_C}^2}$ with $X_C = \frac{1}{\omega C}$. Inserting this into the previous expression yields the final result, which is proportional to the normalised change of the plasmon frequency:

$$\left|\frac{\Delta Q}{Q}\right| = \frac{1}{\sqrt{(RC\omega)^2 + 1}} \propto \frac{\Delta\omega}{\omega}. \tag{S3}$$

Introducing the proportionality parameter b and the RC time constant $\tau_{RC} = RC$ yields:

$$\frac{b}{\sqrt{(\tau_{RC}\omega)^2 + 1}} = \frac{\omega(G) - \omega(G=0)}{\omega(G=0)}. \tag{S4}$$

Replacing the frequencies on the right-hand side by their corresponding wavelengths and simplifying the resulting equation yields:

$$\frac{b}{\sqrt{(\tau_{RC}\omega)^2 + 1}} = \frac{\lambda(G=0)}{\lambda(G)} - 1. \tag{S5}$$

Rearranging yields the final result (equation 1, main text):

$$\lambda(G) = \frac{\lambda(G=0)}{\frac{b}{\sqrt{(\tau_{RC}\omega)^2 + 1}} + 1}. \tag{S6}$$

S3. Electromagnetic simulations

Figure S2 a&b show the resulting dependencies of the coupled plasmon mode on both the refractive index and the spacer thickness within the gap. The simulations show that the thickness difference, observed by ellipsometry (see main text), cannot account for the observed blue-shift.

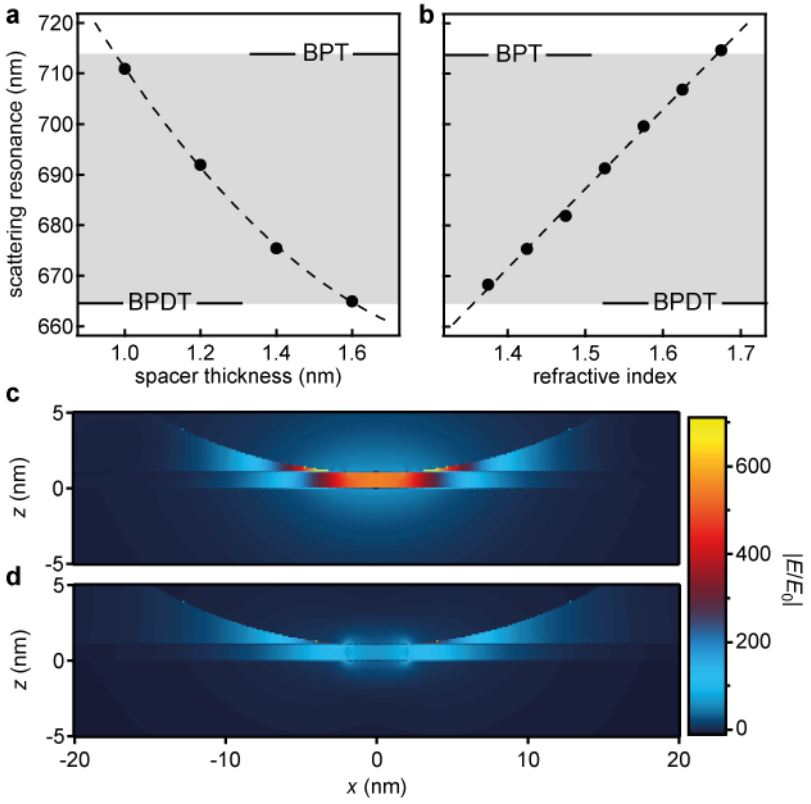

Figure S2 | Electromagnetic simulations of the nanoparticle on mirror geometry. a, resonance wavelength of the coupled plasmon resonance *vs* spacer thickness (*n* = 1.475). **b,** Resonance wavelength *vs* refractive index (spacer thickness = 1.3 nm). The grey areas indicate the experimentally observed blue-shift. **c & d,** Simulated field profiles for an insulating and conducting spacer, respectively.

The simulated near field profiles (Figure S2c,d) demonstrate the reduction of the field enhancement for conductive spacers. This reduction results in a lower Raman signal, as observed experimentally (see main text). To quantify the decrease of the field enhancement we integrate over the area of the hotspot within the spacer layer. As the Raman photons are spectrally shifted with respect to the incoming photon we correct the scattering cross-section S at the respective frequencies of the plasmon resonance (ω_{P}) and the Raman scattered photon (ω_{Laser}- $\Delta\omega_{\mathrm{SERS}}$):

$$\text{Raman enhancement} = \left|\frac{E}{E_0}\right|^2 \times \left|\frac{E}{E_0}\right|^2 \frac{S(\omega_{\mathrm{p}}\text{-}\,\Delta\omega_{\mathrm{SERS}})}{S(\omega_{\mathrm{P}})} \qquad \text{(S7)}$$

From this estimate we expect a 140-fold decrease of the Raman signal in the conducting case.

S4. SERS reference measurements

To demonstrate the Raman enhancement is due to the coupled plasmon modes in the nanoparticle on mirror geometry, Raman maps of a sparsely covered sample were recorded. Fig. S3a shows that a Raman signal can be observed only on the nanoparticles. Away from the nanoparticles no Raman signal is observed (off-nanoparticle spectrum in Fig. S3c shows background noise level). The corresponding dark field image (Fig. S3b) confirms the presence of nanoparticles at the positions with a large Raman enhancement. A linear dependence of the Raman intensity I_{SERS} on the laser power P was observed (Fig. S3d).

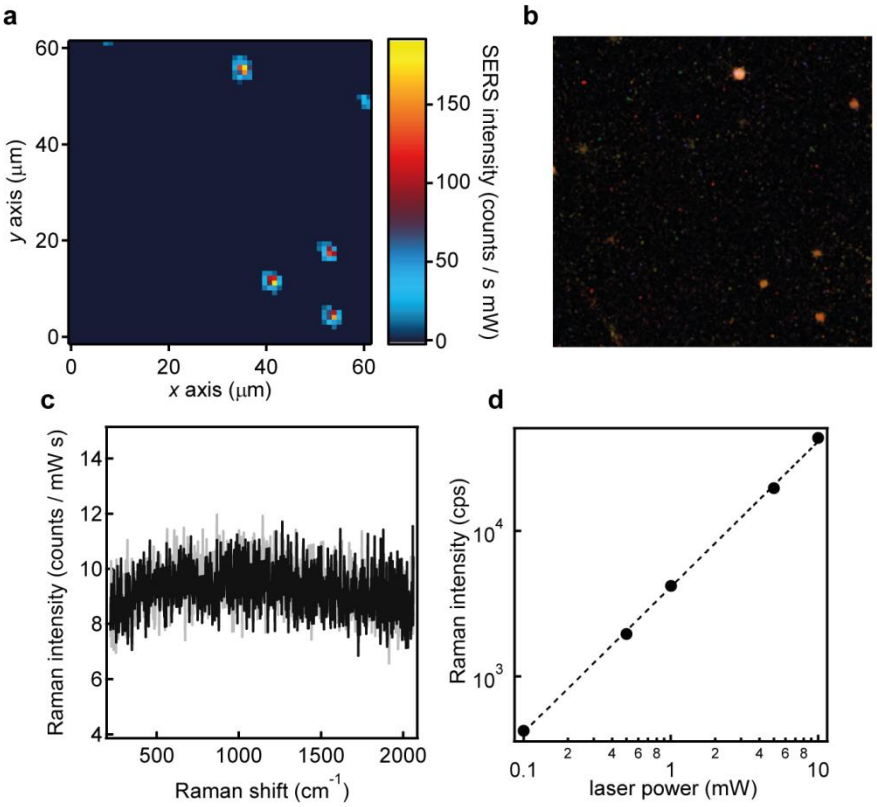

Figure S3 | Reference Raman measurements for BPDT. a, Raman mapping of nanoparticles on a BPDT SAM (633 nm laser, 1 s integration time, 0.33 mW laser power). The colour corresponds to the intensity of the coupled ring vibration a 1585 cm^{-1}. **b,** Corresponding dark field image of the mapped area. **c,** Raman spectra recorded >20μm from a nanoparticle. **d,** Power dependence of the observed SERS signal on an individual nanoparticle.

S5. SERS intensity corrections

For different plasmon resonance wavelengths Raman modes can experience different enhancements. Pivotal is the near-field intensity at the laser frequency (ω_{Laser}), enhancing the incoming photon field, and the near-field intensity at the frequency of the Raman scattered photon (ω_{Laser}- $\Delta\omega_{\mathrm{SERS}}$). These near-field intensities are to first approximation proportional to the scattering strength S at the corresponding wavelengths (Fig. S4). Thus the corrected SERS intensity $\bar{I}_{SERS}$ can be approximated by:

$$\bar{I}_{\mathrm{SERS}} = \frac{I_{\mathrm{SERS}}}{S(\omega_{\mathrm{Laser}}) \times S(\omega_{\mathrm{Laser}} - \Delta\omega_{\mathrm{SERS}})} \tag{S8}$$

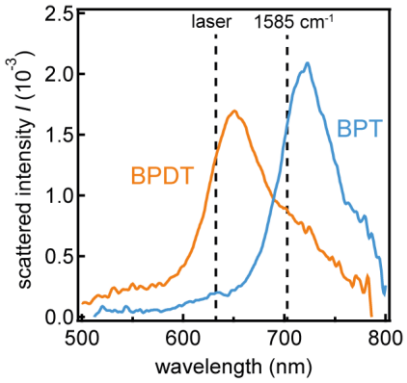

Figure S4 | Example darkfield spectra of gold nanoparticles on BPT and BPDT. Representative dark-field spectra for an individual nanoparticle on mirror, spaced by either BPT or BPDT SAM. The dashed lines indicate the positions of the Raman laser and the outgoing wavelength for a Raman shift of 1585 cm^{-1}.

We have fitted the SERS peak amplitude of the coupled ring mode and corrected the resulting integrated intensities according to equation S6 for all nanoparticles. We find that the intensity ratio of BPT to BPDT is 2.4.

S6. SERS time evolution and correlation analysis

The stability of the SAMs under measurement conditions was tested by recording a time series of Raman spectra with 1 s integration time each. The resulting spectral map is shown in Fig. S5a. For a laser power of 0.33 mW, no photobleaching of the molecules could be observed on the time scale of the measurements. Plotting the spectral shift of the coupled ring mode (1585 cm^{-1}) *vs* the spectral shift of the C-H rocking mode further demonstrates the stability of the modes, as minimally small fluctuations around ± 2 cm^{-1} are seen, which are within the fit uncertainty of the peak position for the present noise. The shape of the fitted 2D Gaussian correlation contour indicates that the mode shifts are not correlated (for a completely correlated change a linear behaviour is expected, a circular shape indicates random shifts of the two modes). This is expected when averaging over the few hundred molecules which hides small changes of individual molecule conformation.

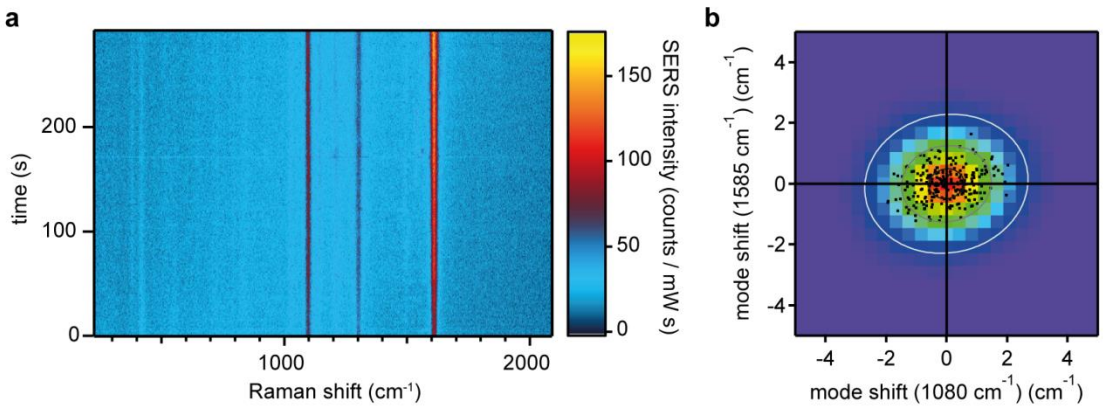

Figure S5 | Time-resolved Raman spectra of an individual nanoparticle on mirror. a, SERS time-series recorded on an 60 nm gold nanoparticle on mirror spaced by a BPDT SAM. 633 nm laser, 0.33 mW, 1 s integration time. **b,** Spectral shift of the coupled ring mode and the C-H rocking mode at different times**.** The grey lines are contour lines of a fitted 2D Gaussian curve; the background image shows the point density.

S7. Linewidth of the coupled plasmon mode

From previous simulations it is known that with increasing conductivity the coupled plasmon mode initially broadens. Starting from a certain threshold on the linewidth starts to decrease as the screened coupled mode is formed.[S1] Figure S6 shows the experimentally observed linewidths (a, averaged from 100 spectra) for different BPDT mole fractions together with the simulated linewidths (b). These simulations capture well the increase and decrease of the FWHM as the molecular conduction turns on.

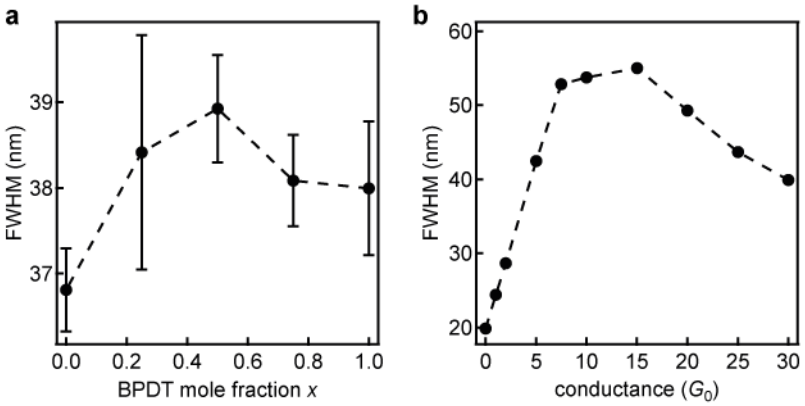

Figure S6 | Full width at half maximum (FWHM) of the coupled plasmon mode. a, Plasmon linewidth for different BPDT mole fractions showing the initial increase and subsequent decrease of the FWHM. Averaged from 100 spectra per point. **b,** FWHM extracted from the electromagnetic simulations.

References

S1. Pérez-González, O. *et al.* Optical Spectroscopy of Conductive Junctions in Plasmonic Cavities. *Nano Lett.* **10,** 3090–3095 (2010).